A Kinematic Source Time Function Compatible With Earthquake Dynamics

Tinti E.[1], Fukuyama E.[2], Piatanesi A.[1], and Cocco M.[1]

March 9, 2005

Submitted to Bullettin of Seismological Society of America

[1] Istituto Nazionale di Geofisica e Vulcanologia, Department of Seismology and Tectonophysics, Via di Vigna Murata 605, Rome, 00143, Italy

[2] National Research Institute for Earth Science and Disaster Prevention, 3-1 Tennodai, Tsukuba, 305-0006, Japan

Abstract

We propose a new source time function to be used in kinematic modeling of ground motion time histories, which is consistent with dynamic propagation of earthquake ruptures and makes feasible the dynamic interpretation of kinematic slip models. This function is derived from a source time function first proposed by Yoffe (1951), which yields a traction evolution showing a slip-weakening behavior. In order to remove its singularity we apply a convolution with a triangular function and obtain a regularized source time function called "regularized Yoffe" function. We propose a parameterization of this slip velocity time function through the final

slip, its duration and the duration of the positive slip acceleration (T_{acc}). Using this analytical function we examined the relation between kinematic parameters, such as peak slip velocity and slip duration, and dynamic parameters, such as slip weakening distance and breakdown stress drop. The obtained scaling relations are consistent with those proposed by Ohnaka and Yamashita (1989) from laboratory experiments. This shows that the proposed source time function is suitable to represent the dynamic rupture propagation with finite slip-weakening distances.

1 Introduction

Kinematic rupture models for moderate to large earthquakes are currently obtained by inverting ground motion waveforms, which provide a detailed image of the slip history during the rupture process (e.g. Hartzell and Heaton, 1983; Fukuyama and Irikura, 1986; Takeo, 1987; Beroza and Spudich, 1988; Yoshida and Koketsu, 1990; Wald and Heaton, 1994; Yoshida et al., 1996; Cotton and Campillo, 1995; Yagi and Kikuchi, 2000; Bouchon, et al., 2000; Sekiguchi and Iwata, 2002 among many others). One fundamental purpose of these inverse modeling attempts is to improve our understanding of the physical processes governing dynamic rupture propagation and the seismic wave generation. It is still an important task to distinguish between different slip models characterized by a propagating slip pulse (Heaton, 1990; Zheng and Rice, 1998) or a crack-like rupture growth (Das and Aki, 1977; Day 1982). Kinematic source models retrieved through the inversion of seismological and geodetic data have shown that large slip patches are usually a small fraction of total rupture area. Slip heterogeneity and rupture complexities are probably generated by a combination of different factors such as non-uniform initial stress

distributions, non-planar fault geometry and heterogeneous distribution of constitutive properties of the fault as well as of the elastic properties of the crust.

Several assumptions are needed to constrain the rupture history of an earthquake and to infer a unique kinematic source model whose simulated waveforms have reasonable fit to observations. We do not discuss here the issues related to the discrete representation of the fault as well as to the resolution and the accuracy of the inversion procedure. Instead, we will focus on the adoption of the source time function (STF) that prescribes the slip velocity evolution during the rupture propagation on the assumed fault. This is particularly important for single time-window inversion procedures, in which the temporal evolution of slip or slip velocity is prescribed by assuming an analytical expression of STF. However, multi-window approaches are often applied to invert ground motion time histories. The STF adopted in multi-window methods are rather crude and the final source time function is given by the superposition of several functions (a triangular function in most of the cases) appropriately shifted in time. Cohee and Beroza (1994) compared these two methods of waveform inversion and found that the single time window technique does a better job in recovering the true seismic moment and the average rupture velocity.

Nakamura and Miyatake (2000) proposed an "ad hoc choice" of the slip velocity function to fit dynamic rupture models. In their time-domain parametrization they introduced a source time function composed by the combination of a quadratic function, a kostrov function and finally a linear function. They were interested in near-field strong ground motion simulations rather than to better constrain the dynamic models. Several others papers (Hisada, 2000; 2001; Guatteri et al., 2003) have pointed out the importance of the STF in kinematic source models for strong ground motion prediction.

Nielsen and Madariaga (2003) theoretically derived a formulation for self-similar and self-healing pulses, which may represent an alternative to the Kostrov's crack solution (i.e., a square root singularity function; Kostrov, 1964) and is compatible with evidences of pulse-like rupture propagation observed in many investigations (e.g. Heaton, 1990). This function was originally proposed by Yoffe (1951) for steady state solution in mode I crack and subsequently by Broberg (1978, 1999) and Freund (1979), who extended it to a mode II crack propagation. In this paper we refer to this source time function as the *Yoffe* function. Piatanesi et al. (2004) discussed the effect of different STFs on the estimation of dynamic parameters. In particular, they compared the traction evolutions inferred from several well-known STFs: a smoothed ramp function, an exponential function and a regularized *Yoffe* function (see some examples in Figure 1). They pointed out that the distribution of dynamic parameters strongly depends on the assumed STF and they suggested that the obtained dynamic parameters might be biased especially when using STFs that are not compatible with elastodynamics. In particular, these authors have shown that the inferred values of the critical slip weakening distance, stress drop and strength excess as well as their distribution on the fault plane are affected by the adopted source time function.

In this paper, we extend the work by Piatanesi et al. (2004) by introducing a new STF and providing an analytical form which is compatible with elastodynamics. We propose an analytical function which is suitable for the dynamic rupture modeling based on the *Yoffe* function derived by Nielsen and Madariaga (2003). In order to eliminate its singularity, we convolve the original *Yoffe* function with a triangular function and obtain a regularized *Yoffe* function. We promote our solution for several reasons. First, this

function is consistent with the self-similar solution of elastodynamic equation and with spontaneous dynamic models governed by slip-weakening (Nielsen and Carlson, 2000; Nielsen and Madariaga, 2003). Second, this function can describe a local healing process with variable rise time consistent with laboratory experiments on fault friction (Ohnaka and Yamashita, 1989). Third, this function is consistent with traction evolution of spontaneous crack models, describing the traction drop near the propagating rupture front within the cohesive zone and providing realistic values of the critical slip weakening distance. Fourth, this function can be easily used in either forward or inverse waveform modeling.

2 Kinematic source time function

2.1 Analytical form of the new source time function

The most common assumption in kinematic modeling of ground motion time histories is the definition of a finite slip duration during the rupture propagation at variable velocity (e.g. Heaton, 1990). Once the source time function is chosen, its shape is prescribed by the total slip value, the rupture time and the rise time (duration of slip) at each point on the fault. This parameterization is common to both multi-window and single window inversion procedures. However, the former approach allows in principle a more flexible way of modeling slip duration (e.g. Hartzell and Heaton, 1983; Wald and Heaton, 1994; Yagi and Kikuchi, 2000; Sekiguchi and Iwata, 1996; Kaverina et al., 2002). If the temporal resolution would be high (i.e. very short duration of unit source time functions), the multi-window approach might yield reasonable estimations of total slip duration. Unfortunately,

this condition is very rare and for most of the applications the total slip duration at each point on the fault is inferred through a few (less than 6) superimposed simple functions. The single window approach has been used by assuming different functional forms of STF to retrieve the rupture history of large earthquakes (e.g. Fukuyama and Irikura, 1986; Fukuyama and Mikumo, 1993; Cotton and Campillo, 1995). The more unphysical STF is the Heaviside function in slip, corresponding to a delta function in slip velocity. The simplest STF is a ramp in slip of duration τ_R (its corresponding slip velocity is a box-car) and a smoothed ramp function proposed by Bouchon (1997) (its corresponding slip velocity is similar to a Gaussian function). More complicated functions have been proposed: the truncated inverse square root singularity (Beroza and Spudich, 1988), the exponential (Cotton and Campillo, 1995) and the power law (Liu and Archuleta, 2004) functions among many others. In Figure 1 we show examples of these functions. In many of the above studies, the selection of STF was done without careful inspections on the physical consistency nor insights to the consequences for dynamic modeling.

Following Piatanesi et al (2004), we deal in this work with the problem of kinematic models consistent with earthquake dynamics. To this goal we propose a regularized *Yoffe* function as a candidate of a kinematic source time function. Nielsen and Madariaga (2003) proved that the *Yoffe* function shown in Equation (1) is an alternative of the Kostrov solution (Kostrov, 1964).

$$Y(t) = \frac{2}{\pi\tau_R} H(t)H(\tau_R - t)\sqrt{\frac{\tau_R - t}{t}} \tag{1}$$

where τ_R is the rise time and $H(t)$ is the Heaviside function. Thus we modified this analytical *Yoffe* function as described in Equation (1) in order to remove the singularity

at the rupture front. Piatanesi et al. (2004) showed that if the *Yoffe* function is convolved with a triangular time function, the source time function can be used as a boundary condition in a 3D dynamic rupture computation to compute the traction evolution. The constitutive relation inferred from both assumed slip function and corresponding traction evolution still preserves a slip-weakening behavior as the original *Yoffe* function. Here we derive an explicit form of this function by analytical computation. The triangular function can be expressed as follows:

$$W(t) = \frac{1}{\tau_S^2}\left[tH(t)H(\tau_S - t) + (2\tau_S - t)H(t - \tau_S)H(2\tau_S - t)\right] \tag{2}$$

where τ_S is the half duration of the triangular function. Therefore, the regularized *Yoffe* function can be obtained by convolving Equation (1) with Equation (2) as follows:

$$S(t) = D_{max}\int_{-\infty}^{+\infty} W(t - T)Y(T)dT \tag{3}$$

where D_{max} stands for final slip. The explicit analytical formulation of this function is presented in the Appendix. In the following of this study we refer to $S(t)$ as a slip velocity time function. It should be noted that the regularized *Yoffe* function can now be fully described through three parameters: τ_R, τ_S, and D_{max}. In Figure 2 we show a comparison between the original *Yoffe* function and the regularized *Yoffe* proposed in this study.

In the following sections we investigate the relations between these three parameters and those obtained by dynamic rupture computations. This allows us to investigate the fundamental features of the key kinematic parameters useful to describe the source process. It should also be noted that this function is similar to that inferred by Ohnaka and Yamashita (1989) from laboratory experiments (see Panel C in Figure 6 of Ohnaka and Yamashita, 1989).

2.2 Parameterization of source time function

Numerical simulations of spontaneous dynamic rupture of earthquakes clearly show that the traction evolution within the cohesive zone controls the slip acceleration and the slip velocity time history (Bizzarri and Cocco, 2003; Cocco et al., 2004 and reference therein). Recent investigations have pointed out that the shape, peak value and time of peak slip velocity vary during the dynamic propagation. These parameters are controlled by the initial stress, frictional parameters and constitutive relations on the fault.

It seems convenient to introduce a new parameter T_{acc}, which is defined as the time to peak slip velocity (i.e. the duration of positive slip acceleration) as illustrated in Figure 2. In the original *Yoffe* function, T_{acc} is zero because of the singularity. On the contrary, in the regularized *Yoffe* function, T_{acc} is controlled by the duration of the triangular function used as a smoothing operator τ_S, which is not a physical parameter. The temporal smoothing of original Yoffe function yields finite peak slip velocity values. Because τ_S appears only in the regularized *Yoffe* function, we numerically investigated the relation between T_{acc} and τ_S for different τ_R. As shown in Figure 3, T_{acc} is linearly related to τ_S, confirming that τ_S directly controls the duration of the positive slip acceleration (T_{acc}). In particular, the ratio T_{acc}/τ_S does not depend on other parameters and is equal to 1.27 ± 0.01. The linear relation has been inferred by varying the rise time between 0.2s and 6.0s: Figure 3 clearly shows that τ_S does not affect T_{acc}.

However it should be noted that, after temporal convolution, the effective final duration of the STF (τ_R^{eff}) is slightly larger than τ_R:

$$\tau_R^{eff} = \tau_R + 2\tau_s \tag{4}$$

Therefore, our proposed source time function is parameterized by the three parameters having a clear physical meaning: the total slip D_{max}, the slip duration (rise time) τ_R and the duration of the positive slip acceleration T_{acc}. We will discuss later the relation between these parameters and the dynamic ones which govern the dynamic process of earthquake rupture.

2.3 Kinematic relations

In this section we discuss the relations between the kinematic source parameters: τ_R, D_{max}, T_{acc}, τ_S, and V_{peak}. We start pointing out that only a few parameters are usually retrieved through kinematic analyses of forward or inverse modeling of seismic waves (see Beresnev, 2003). The rupture time, final slip and, sometimes, the slip duration are commonly estimated but slip velocity function and inferred peak slip velocity are rarely estimated. We emphasize, however, that the relation between D_{max} and V_{peak} depends on the adopted source time function. Moreover, V_{peak} can change dramatically during the dynamic rupture process.

We plot in Figure 4 a set of our new STF obtained by changing only the τ_R values (upper panel) or the τ_S values (bottom panel). From Figure 4 we observe that T_{acc} does not depend on the rise time τ_R but is related to τ_S as described above. This is physically reasonable because it is widely believed that different mechanisms control slip acceleration and the healing of slip (see Bizzarri and Cocco, 2003; Cocco et al., 2004, and references therein).

To investigate analytically the relation between T_{acc} and the corresponding V_{peak}, we need to compute the derivative of STF (i.e. slip acceleration function). Since T_{acc} is

always in the range between τ_S and $2\tau_S$ as illustrated in Figure 3, the derivative in this range becomes

$$\dot{S}(t) = -2\sqrt{(t-\tau_S)(\tau_S+\tau_R-t)} - 2\tau_R \arcsin\sqrt{\frac{t-\tau_S}{\tau_R}} + \sqrt{t(\tau_R-t)} + \tau_R \arcsin\sqrt{\frac{t}{\tau_R}} \quad (5)$$

Unfortunately it was quite difficult to find an explicit analytical formulation of T_{acc}, which is the solution of $\dot{S}(t) = 0$. We are therefore confined to solve this equation numerically. We compute the Taylor series expansion of Equation (5) to obtain the expression of T_{acc} as a function of other parameters. The obtained relation is

$$T_{acc} = 1.3\tau_S + O(f(\tau_R, \tau_S)) \quad (6)$$

which is consistent with the numerical results shown in Figure 3. This relation allows us to express V_{peak} as a function of T_{acc}, τ_R, and D_{max}.

We then insert Equation (6) into the solution of Equation (3) presented in the Appendix (Eqs. A13 or A14) for the range $\tau_S < t < 2\tau_S$. V_{peak} might be obtained from this relation for $t = T_{acc}$. Unfortunately, the resulting relation was again complicated and it seems difficult to obtain the explicit formulation of V_{peak} as a function of other kinematic parameters such as T_{acc}, τ_R, and D_{max}. For this reason, we are forced to search the simplest relation numerically, by computing many regularized *Yoffe* functions varying the relevant parameters, as shown in Figure 4. The right panels of Figure 4 display the inverse dependence of V_{peak} on τ_S and τ_R. We then found the following asymptotic relation by trial and error:

$$V_{peak} = 1.04\frac{D_{max}}{(T_{acc})^{0.54}(\tau_R)^{0.47}} \simeq C\frac{D_{max}}{\sqrt{T_{acc}}\sqrt{\tau_R}} \quad (7)$$

Figure 4 shows that the regularized Yoffe functions obtained by fixing the slip duration ($\tau_R = 2.5s$, bottom panels) display different effective durations (τ_R^{eff}) ranging within the interval predicted by Equation (4). Thus, since τ_R is fixed, τ_R^{eff} varies because τ_S is changing. Equation (7) allows the association between final slip and peak slip velocity for a given regularized Yoffe function. It should be noted that T_{acc} is different from T_w proposed by Ohnaka and Yamashita (1989). They introduced T_w as the half width of total slip acceleration (that means half rise time) to connect this kinematic parameter with the dynamic breakdown time (T_c). T_c is defined as the time required for the shear stress to decrease from its peak value to a kinetic frictional stress level. In the dynamic spontaneous rupture models T_c is usually non-uniform on the fault. This parameter defines the duration of breakdown process within the cohesive zone. Ohnaka and Yamashita (1989) related T_c with the cutoff frequency (f_{max}^s) of the power spectral density of slip acceleration of the same point on the fault as $f_{max}^s = 1/T_c$.

We will do something similar with T_{acc} and T_c in the following sections. This new *Yoffe* function allows the slip acceleration to be bounded at and near the propagating crack tip (see panel B in Figure 5). This feature is very important and it is not ensured in dynamic modeling simply introducing a cohesive zone with a constitutive law. The peak slip acceleration is one of the key parameters characterizing earthquake source which is important also for strong ground motion prediction.

3 Deriving dynamic rupture parameters from kinematic models

3.1 Computation method for dynamic rupture

We use a 3-D finite difference code to calculate the stress time history on the earthquake fault plane (Andrews, 1999). The stress is computed through the fundamental elastodynamic equation (Ide and Takeo, 1997). The total dynamic traction in each fault position can be explicitly calculated by the sum of two contributions: the instantaneous term depending on slip velocity and the dynamic load related to the previous slip history. This explicit dependence has been found analytically by Fukuyama and Madariaga (1998). Their inferred equation is the following:

$$\sigma(x,t) = -\frac{\mu}{2\beta}S(x,t) + \int_{\Sigma}\int_{0}^{t} K(x-\xi;t-t')S(\xi,t)dt'dS \tag{8}$$

where $S(x,t)$ represents the slip velocity (STF), β the shear velocity, K the dynamic load associated to those points that are still slipping. We show this formulation only to highlight the direct effect of the local source time function on the corresponding traction evolution. In the present study we impose the slip velocity as a boundary condition. In other words, each node belonging to the fault plane is forced to move with a prescribed slip velocity time history. In this way we do not need to specify any constitutive relation and the dynamic traction evolution is the result of calculation. The space and time distribution of slip velocity is derived from the kinematic rupture models. In this work we use the new regularized STF obtained in the previous section. We assume a homogeneous half-space discretized with grid size $\Delta x = \Delta y = \Delta z = 50m$, time step $\Delta t = 0.005s$, density

$\rho = 2700kg/m^3$ and P- and S- wave velocities are $v_p = 5.2km/s$ and $v_s = 3.0km/s$, respectively. A planar vertical fault is assumed whose dimensions are $12.8km$ along strike and $6.4km$ along dip. The hypocenter is located at 6.4km along strike and 3.2 km along dip, which is the same for all models. Upper margin of the fault is at the free surface.

3.2 Inferred dynamic parameters

We have computed a number of models to examine the relations between kinematic and dynamic parameters as listed in Table 1. All models have a strike slip faulting with a uniform distribution of rupture velocity (v_r), τ_R, T_{acc}, D_{max} and initial stress on the fault plane. This means that at each point on the fault the slip velocity function is the same but shifted along time. On the contrary the traction evolution depends on the position on the fault because of the different contribution of the dynamic load (second term in Equation (8)). In this computation, we did not use the points close to the fault edge to avoid the artificial reflections due the lack of absorbing boundary condition. In Figure 5 we show an example of the inferred traction evolution at an interior point on the fault plane using the proposed new STF and the kinematic parameters of model #5 in Table1: panel A displays the adopted STF, panel B the resulting slip acceleration, panel C the calculated temporal evolution of dynamic traction and panel D illustrates the traction evolution as a function of slip. Since seismic waves are only sensitive to the stress change, we can only discuss the relative values of stress. We treat the following values as relative ones: strength excess (difference between yield stress and initial stress), dynamic stress drop (difference between initial stress and minimum stress during slipping), breakdown stress drop (difference between yield stress and minimum stress, $\Delta\sigma_b$). Therefore, we

need to assume a initial stress (σ_0) distribution to interpret the slip-weakening curves and the distribution of dynamic parameters on the faults (Tinti et al. 2005). In this paper we assume a uniform initial stress distribution to examine more easily the dependence of dynamic and kinematic parameters. Hereafter, we show the stress change evolution relative to the uniform initial stress, i.e. $\sigma(t) - \sigma_0$.

We illustrate in Figure 5(D) the strength excess and the dynamic stress drop at this selected point on the fault. We observe a clear restrengthening of stress associated to the healing of slip in Figure 5(C) and (D). This behavior is called 'undershoot'. We have to note , however, that such a behavior might depend on the position on the fault. In Figure 5(D), the slip weakening behavior is observed with a critical slip weakening distance D_c. Tinti et al. (2005) have shown that the spatial distributions on the fault plane of strength excess and dynamic stress drop are strongly controlled by the adopted kinematic parameters. In particular, the strength excess is affected by rupture time distribution as well as by the peak slip velocity distribution as we will show in the next section, while the dynamic stress drop is controlled mainly by the slip distribution.

4 Relation between kinematic and dynamic source parameters

A common feature of dynamic models is the traction evolution within the cohesive zone showing a slip-weakening behavior, which in general may have variable weakening rate (i.e., not linear). This has been observed in dynamic simulations performed with different constitutive laws, including time weakening or rate and state dependent friction laws

(see Bizzarri and Cocco, 2003 and references therein). The modeling results shown in Figure 5(D) indicate that the peak stress is attained at nonzero slip and that a slip-hardening phase precedes the slip-weakening phase. In our simulations this behavior is a consequence of imposing a bounded slip acceleration. We discuss here that the dynamic traction growth to the upper yield stress value is associated to the slip acceleration phase; in our calculations, the value of T_{acc} controls the traction evolution and the dynamic weakening rate (as seen both by traction versus time and versus slip). In this section we aim to propose useful relations between kinematic and dynamic parameters. We will compare in the following our scaling relations with those proposed by Ohnaka and Yamashita (1989).

We have performed a series of simulations with the parameters listed in Table 1. Each model has a constant rupture velocity and a uniform distribution of kinematic parameters on the fault plane. Figure 6 shows the dynamic traction evolutions and the constitutive behaviors calculated using different slip velocity functions, each of which is obtained by different smoothing factor τ_S; consequently different T_{acc}.

According to Equation (7) we expect the variation of V_{peak} as a function of T_{acc}, which can be seen in the left panel of Figure 6. Looking at the traction time histories and at the constitutive behaviors in Figure 6, we observe that strength excess ($\Delta\sigma_b$), T_c and D_c depend on T_{acc}. In particular, we point out that the weakening rate ($\Delta\sigma_b/D_c$) is associated to T_{acc}, characterizing the adopted source time function.

To examine the relations between kinematic and dynamic parameters we plot the relations of V_{peak} versus D_c and $\Delta\sigma_b$ and T_{acc} versus T_c in Figure 7. We found a negative correlation between V_{peak} and D_c. On the contrary, a positive correlation between V_{peak}

and $\Delta\sigma_b$ is inferred. Besides, the central panel of Figure 6 and the right panel of Figure 7 show a positive correlation between T_{acc} and T_c, i.e. $T_{acc} = kT_c$, where k is a positive constant equal to ~ 0.75 for all models computed in Tabel 1.

We show in Figure 8 the traction evolutions and constitutive behaviors corresponding to several slip velocity functions with different τ_R (and constant T_{acc}). The left panel of this figure indicates that decrease of τ_R reduces the frictional stress level and increases D_c. In particular, looking at the central panel of Figure 8, we observe that the minimum traction is achieved at the same time, which means that T_c is constant. The comparison between the slip-waekening curves (stress versus slip plots) in Figures 6 and 8 confirms that T_{acc} controls the weakening rate ($\Delta\sigma_b/D_c$). The inverse relation between τ_R and D_c in Figure 8 may look somehow strange, but since all the kinematic parameters other than τ_R are kept constant and the inferred T_c is then constant, the shorter τ_R results in the larger D_c. In Figure 9 we plot the V_{peak} versus D_c for four simulations with different uniform τ_R (varying from 1.0s to 3.0s) and for a simulation having variable rise time on the fault ranging from 0.6s to 3.5s. In this case, we observe a positive correlation between these two parameters. This is because D_{max} is kept constant and then shorther τ_R produces larger V_{peak}.

By compiling all these simulations we have verified that V_{peak} is related to D_{max} and D_c by an expression depending on both τ_R and T_{acc}. Here we propose the following scaling relations derived for uniform τ_R and T_{acc}, respectively:

$$V_{peak} \propto \frac{D_{max}^2}{D_c \tau_R} \qquad \text{(for uniform } \tau_R\text{)} \tag{9}$$

$$V_{peak} \propto \frac{D_c}{T_{acc}} \qquad \text{(for uniform } T_{acc}\text{)} \tag{10}$$

From these equations we obtain:

$$D_c \propto \sqrt{\frac{T_{acc}}{\tau_R}} D_{max} \tag{11}$$

Equation (10) is the same as Equation (44) in Ohnaka and Yamashita (1989): $\dot{D}_{max} = (0.56 \sim 0.91) D_c f^s_{max}$, where $\dot{D}_{max}$ is peak slip velocity and f^s_{max} is the inverse of T_c. From this equation, it emerges that the ratio D_c/D_{max} depends on the ratio T_{acc}/τ_R and therefore it can be variable on the fault plane.

We obtain the relation between V_{peak} and breakdown stress drop:

$$V_{peak} \propto \Delta\sigma_b \tag{12}$$

This equation corresponds to the Equation (47) of Ohnaka and Yamashita (1989) ($\dot{D}_{max} = v\sigma_p/C(v)\mu$, where σ_p is $\Delta\sigma_b$ in our notation and μ is the rigidity). Finally, from Equations (10) and (12) as well as the relation $T_{acc} \propto T_c$, we obtained $T_c \propto D_c/\Delta\sigma_b$, that is the same as Equation (50) of Ohnaka and Yamashita (1989).

In all the above proposed scaling relations we can consider the dependence of rupture velocity. We examined the effect of variable rupture velocity (different uniform rupture time distribution). By fixing D_{max}, T_{acc} and τ_R (then V_{peak} becomes fixed), we simulated rupture processes changing only the rupture time distribution. The range of rupture velocity (v_r) is set from 1.5 km/s to 3.0 km/s. We plot the corresponding traction evolutions and the inferred constitutive behaviors for the same point on the fault in Figure 10. Because in our simulations the rupture onset (i.e. the rupture times, tr) are different, in

central panel we plot $\Delta\sigma$ as a function of relative time $(t - tr)$. D_c and T_c are approximatively constant and the variation between the traction evolutions depends only on $\Delta\sigma_b$. From Figure 11, we found an inverse correlation between $\Delta\sigma_b$ and v_r. In these simulations V_{peak} is set constant. We confirmed that Eq. (12) becomes

$$V_{peak} \propto C(v_r)\Delta\sigma_b \tag{13}$$

where $C(v_r)$ is a constant depending on the rupture velocity, as stated in the Ohnaka and Yamashita (1989) equations.

5 Discussions

In this study we propose an innovative and original parameterization of the source time function to be used in kinematic modeling of ground motion time histories. We suggest that a kinematic model can be adequately described by the total slip (D_{max}) and the rupture time distributions on the fault plane as well as by the source time function defined by the slip duration (τ_R) and the duration of the positive acceleration (T_{acc}). We have proposed several scaling relations between kinematic and dynamic parameters. It is important to emphasize that our proposed scaling relations agree with those obtained by Ohnaka and Yamashita (1989). Their work is based on a comparison between laboratory experiments, theoretical considerations and numerical simulations of spontaneous dynamic crack propagation in 2-D. They assumed a slip-dependent constitutive law (exponential law) and inferred some relations between kinematic and dynamic parameters. Moreover, their theoretical and numerical results start from the crack model assumption, not including the local healing of slip. Our assumptions are completely different

but the inferred relations are consistent. Because our slip velocity functions have a finite duration, the inferred traction evolution shows restrengthening and healing of slip. The agreement between our scaling relations and those proposed by Ohnaka and Yamashita (1989) further corroborates the validity of our numerical analyses.

We have shown in this study that the parameter T_{acc}, used to define the regularized Yoffe function here proposed, is linearly related to the duration of the breakdown process T_c (see Figures 5 and 6) and that the proportionality factor between these two parameters depends on the assumed rupture velocity. This is evident looking at the results of our simulations listed in Table 1. Mikumo et al. (2003) proposed that the critical slip weakening distance can be measured as the slip at the time of peak slip velocity. This implies that the duration of the positive slip acceleration T_{acc} has to be close to the duration of the breakdown process, and thus their ratio should be close to unity. Our modeling results suggest that this is true only for constant (or weakly variable) rupture velocity models. More recently, Tinti et al. (2004) have shown that T_{acc} and T_c depend on the adopted constitutive law and on the constitutive parameters as well as the friction behavior at high slip rates. Therefore, we emphasize that T_{acc} is a source parameter with a clear physical meaning and it is directly controlled by fault constitutive properties. Simulations with spontaneous dynamic rupture models suggest that in general T_{acc} can change on the fault plane.

Another interesting result of our study is the linear relation between peak slip velocity and breakdown stress drop, in agreement with Ohnaka and Yamashita (1989). This scaling relation points out that peak slip velocity is related to the mechanisms controlling the breakdown process and to the earthquake stress drop. The proportionality factor

bewteen these two parameters depends on rupture velocity, as previously suggested by Ohnaka and Yamashita (1989). We have also shown that the final slip (D_{max}) and the critical slip weakening distance D_c are related and that their ratio depends on both slip duration and T_{acc}. This scaling relation (see Equation 11) does not imply that the ratio between these two parameters is constant on the fault plane, because both T_{acc} and τ_R can vary as a function of positions on the fault plane.

The scaling relations proposed in this study can be very useful to constrain the values and to potentially reduce the number of independent parameters in the kinematic inversion of seismograms. For example, once we construct a model with a given distribution of D_{max} and D_c, we can examine the different combinations of other parameters such as τ_R and V_{peak}. It should be emphasized that in many kinematic models τ_R is not well constrained and T_{acc} is not investigated and imposed along with the assumed source time function. Although we believe that the estimation of T_{acc} through the modeling of radiated waveforms is extremely delicate, we underline that the proposed parameterization of the STF is suitable to associate kinematic and dynamic parameters. This is very important for the dynamic interpretation of kinematic slip models.

6 Conclusions

In this study we proposed an analytical expression of a source time function compatible with dynamic rupture simulations (Nielsen and Madariaga, 2003; Piatanesi et al., 2004). This slip velocity function is based on the function proposed by Yoffe (1951), and subsequently by Broberg (1978) and Freund (1979). We regularized the function by applying

a smoothing operator (i.e., a triangular function with a duration of $2\tau_S$). By varying τ_S, we generated a family of source time functions having different peak slip velocities and slip durations (τ_R^{eff}). We showed that this new slip velocity function, which is described by three parameters: the final slip D_{max}, the slip duration (i.e. rise time) τ_R and the duration of the positive slip acceleration (i.e. time to peak slip velocity) T_{acc}. This slip velocity function is very useful in kinematic modeling of ground motion and allows an easy implementation in numerical codes. We have finally derived a scaling relation between V_{peak} and the three kinematic parameters D_{max}, T_{acc} and τ_R as shown in Equation 8.

We used the 3-D finite difference dynamic code to retrieve the dynamic traction evolution from the slip velocity history by imposing slip velocity as a boundary condition on the fault plane. We have performed many simulations using different kinematic models with different source time functions. By analyzing the results of our simulations we obtained scaling relations between V_{peak} and relevant dynamic parameters as well as the scaling between D_c and D_{max} at each point on the fault. Our results are of relevance to both kinematic modeling of ground motion time histories and the parameterization of kinematic slip models. The usage of this slip function guarantees the estimation of the temporal evolution of dynamic parameters.

References

Andrews, D. J. (1999) Test of two methods for faulting in finite-difference calculations, *Bull. Seismol. Soc. Am.*, **89**, 931-937.

Beresnev I.A.(2003) Uncertainties in finite-fault slip inversions: To what extent to be-

lieve? (A critical review), *Bull. Seismol. Soc. Am.*, **93**,2445-2458.

Beroza, G. C. and P. Spudich (1988) Linearized inversion for fault rupture behavior: Application to the 1984 Morgan Hill, California, earthquake, *J. Geophys. Res.*, **93**, 6275-6296.

Bizzarri, A. and M. Cocco (2003) Slip-weakening behavior during the propagation of dynamic ruptures obeying rate- and state-dependent friction laws, *J. Geophys. Res.*, **108**, 2373, doi:10.1029/ 2002JB002198.

Bouchon, M. (1997) The state of stress on some faults of the San Andreas system as inferred from near-field strong motion data, *J. Geophys. Res.*, **102**, 11731-11744.

Bouchon, M., N. Toksoz, H. Karabulut, M.-P. Bouin, M. Dietrich, M. Akter, M. Edie (2000) Seismic imaging of the 1999 Izumit (Turkey) rupture inferred from the near-fault recordings, *Geophys. Res. Lett.*, **27**, 3013-3016.

Broberg, K. (1978) On transient sliding motion, *Geophys. J. Roy. astr. Soc.*, **52**, 397-432.

Broberg, K. (1999) *Cracks and Fracture*, Academic Press, New York.

Cocco, M., A. Bizzarri, and E. Tinti (2004) Physical interpretation of the breakdown process using a rate- and state-dependent friction law, *Tectonophys.*, **378**, 241-262.

Cohee, B. P. and G. C. Beroza (1994) A comparison of two methods for earthquake source inversion using strong motion seismograms, *Ann. Geophys.*, **37**, 1515-1538.

Cotton, F. and M. Campillo (1995) Frequency domain inversion of strong motions: Application to the 1992 Landers earthquake, *J. Geophys. Res.*, **100**, 3961-3976.

Das, S. and Aki, K. (1977) A numerical study of two-dimensional spontaneous rupture propagation, *Geophys. J. R. Astr. Soc.*, **50**, 643-668.

Day, S. (1982) Three-dimensional finite-difference simulation of fault dynamics: rectangular faults with fixed rupture velocity, *Bull. Seismol. Soc. Am.*, **72**, 705-727.

Freund, L. B. (1979) The mechanics of dynamic shear crack propagation, *J. Geophys. Res.*, **84**, 2199-2209.

Fukuyama, E. and K. Irikura (1986) Rupture process of the 1983 Japan Sea (Akita-Oki) earthquake using a waveform inversion method, *Bull. Seismol. Soc. Am.*, **76**, 1623-1649.

Fukuyama, E. and R. Madariaga (1998) Rupture dynamics of a planar fault in a 3D Elastic medium: Rate- and slip- weakening friction, *Bull. Seismol. Soc. Am.*, **88**, 1-17.

Fukuyama, E. and T. Mikumo (1993) Dynamic rupture analysis: Inversion for the source process of the 1990 Izu-Oshima, Japan, earthquake (M=6.5), *J. Geophys. Res.*, **98**, 6529-6542.

Guatteri, M., P. M. Mai, G. C. Beroza, and J. Boatwright (2003) Strong ground-motion prediction from stochastic-dynamic source models, *Bull. Seismol. Soc. Am.*, **93**, 301-313.

Hartzell, S. H. and T. H. Heaton (1983) Inversion of strong ground motion and teleseismic waveform data for the fault rupture history of the 1979 Imperial Valley, California, earthquake, *Bull. Seismol. Soc. Am.*, **73**, 1553-1583.

Heaton, T. H. (1990) Evidence for and implication of self-healing pulses of slip in earthquake rupture, *Phys. Earth Planet. Interi.*, **64**, 1-20.

Hisada,Y. (2000) A theoretical omega-square model considering the spatial variation on slip and rupture velocity, *Bull. Seismol. Soc. Am.*, **90**, 387-400.

Hisada,Y. (2001) A theoretical omega-square model considering the spatial variation on slip and rupture velocity.II. Case for a two-dimensional source model, *Bull. Seismol. Soc. Am.*, **91**, 651-666.

Ide, S. and M. Takeo (1997) Determination of constitutive relations of fault slip based on seismic wave analysis, *J. Geophys. Res.*, **102**, 27379-27391.

Kaverina, A., D. Dreger and E. Price (2002) The combined inversion of seismic and geodetic data for the source process of the 16 October 1999 Mw 7.1 Hector Mine, California, earthquake, *Bull. Seismol. Soc. Am.*, **92**, 1266-1280.

Kostrov, B. V. (1964) Self-similar problems of propagation of shear cracks, *J. Appl. Math. Mech.*, **28**, 1077-1087.

Liu, P. and R.J. Archuleta (2004) A new nonlinear finite fault inversion with three-dimensional Green's functions: Application to the 1989 Loma Prieta, California, earthquake, *J. Geophys. Res.*, **109**, 2318, doi:10.1029/ 2003JB002625.

Mikumo, T., K. B. Olsen, E. Fukuyama, and Y. Yagi (2003) Stress-breakdown time and slip-weakening distance inferred from slip-velocity functions on earthquake faults, *Bull. Seismol. Soc. Am.*, **93**, 264 - 282.

Nakamura, H., and T. Miyatake (2000) An approximate expression of slip velocity time functions for simulation of near-field strong ground motion, *Zishin(J. Seism. Soc. Jpn.)*, **53**, 1-9 (in Japanese with English abstract).

Nielsen, S. and J. M. Carlson (2000) Rupture pulse characterization: Self-healing, self-similar, expanding solutions in a continuum model of fault dynamics, *Bull. Seismol. Soc. Am.*, **90**, 1480-1497.

Nielsen, S. and R. Madariaga (2003) On the self-healing fracture mode, *Bull. Seismol. Soc. Am.*, **93**, 2375-2388.

Ohnaka, M. and T. Yamashita (1989) A cohesive zone model for dynamic shear faulting based on experimentally inferred constitutive relation and strong motion source parameters, *J. Geophys. Res.*, **94**, 4089-4104.

Piatanesi, A., E. Tinti, M. Cocco, and E. Fukuyama (2004) The dependence of traction evolution on the earthquake source time function adopted in kinematic rupture models, *Geophys. Res. Lett.*, **31**, L04609, doi:10.1029/ 2003GL019225.

Sekiguchi, H. and T. Iwata (2002) Rupture process of the 1999 Kocaeli, Turkey, earthquake estimated from strong-motion waveforms, *Bull. Seismol. Soc. Am.*, **92**, 300-311.

Takeo, M. (1987) An inversion method to analyse the rupture process of earthquakes using near-field seismograms, *Bull. Seismol. Soc. Am.*, **77**, 490-513.

Tinti E. A. Bizzarri, A. Piatanesi, M. Cocco (2004) Estimates of slip weakening distance for different dynamic rupture models *Geophys. Res. Lett.*, **31**, L02611, doi:10.1029/2003GL018811.

Tinti E., P. Spudich, M. Cocco (2005) Earthquake fracture energy inferred from kinematic rupture models, *submitted to J. Geophys. Res.*.

Wald, D. J. and T. H. Heaton (1994) Spatial and temporal distribution of slip for the 1992 Landers, California, earthquake, *Bull. Seismol. Soc. Am.*, **84**, 668-691.

Yagi, Y. and M. Kikuchi (2000) Source rupture process of the Kocaeli, Turkey, earthquake of August 17, 1999, obtained by joint inversion of near-field data and teleseismic data, *Geophys. Res. Lett.*, **27**, 1969-1972.

Yoffe, E. (1951) The moving Griffith crack, *Phil. Mag.*, **42**, 739-750.

Yoshida, S. and K. Koketsu (1990) Simultaneous inversion of waveform and geodetic data for the rupture process of the 1984 Naganoken-Seibu, Japan, earthquake, *Geophys. J. Int.*, **103**, 355-362.

Yoshida, S., K. Koketsu, B. Shibazaki, T. Sagiya, T. Kato, Y. Yoshida (1996) Joint inversion of near-and far-field waveforms and geodetic data for the rupture process of the 1995 Kobe earthquake, *J. Phys. Earth*, **44**, 437-454.

Zheng, G. and J. R. Rice (1998) Conditions under which velocity-weakening friction

allows a self-healing versus a crack-like mode of rupture *Bull. Seismol. Soc. Am.*, **88**, 1466-1483.

Appendix

We compute the convolution of the original *Yoffe* function $Y(t, \tau_R)$ defined in Equation (1) with the triangular function $W(t, \tau_S)$ defined in Equation (2). The new analytical STF stated in Equation (3) can be expressed as

$$S(t) = D_{max} \int_{-\infty}^{+\infty} W(t - T; \tau_S) Y(T; \tau_R) dT = D_{max}(S1(t) + S2(t)) \tag{A1}$$

where

$$\begin{aligned} S1(t) &= \int_{-\infty}^{+\infty} H(t - T) H(\tau_S - t + T) \frac{t - T}{\tau_S^2} \\ &\quad \times \left[H(T) H(\tau_R - T) \frac{2}{\pi \tau_R} \sqrt{\frac{\tau_R - T}{T}} \right] dT \end{aligned} \tag{A2}$$

$$\begin{aligned} S2(t) &= \int_{-\infty}^{+\infty} H(t - T - \tau_S) H(2\tau_S - t + T) \frac{2\tau_S - t + T}{\tau_S^2} \\ &\quad \times \left[H(T) H(\tau_R - T) \frac{2}{\pi \tau_R} \sqrt{\frac{\tau_R - T}{T}} \right] dT \end{aligned} \tag{A3}$$

There are some different intervals to define the solution. The *Yoffe* function $Y(t)$ is defined in $0 < t < \tau_R$. The triangular function $(W(t))$ has the following two ranges:

1. $t - 2\tau_S < T < t - \tau_S$

2. $t - \tau_S < T < t$

These ranges are represented by the Heaviside functions. Then we compute the integration taking into account the above ranges. When we substitute the integration intervals we have also to consider the *Yoffe* function ranges ($0 < t < \tau_R$). We use the known integral solution:

$$\int x \sqrt{\frac{x}{a - x}} dx = -\frac{2x + 3a}{4} \sqrt{ax - x^2} + \arctan \sqrt{\frac{x}{a - x}} \tag{A4}$$

$$\int \sqrt{-\frac{x+b}{x+a}}dx = \sqrt{-(x+a)(x+b)} + (a-b)\arcsin\sqrt{\frac{x+a}{a-b}} \qquad (a>b) \tag{A5}$$

For the first range ($t - 2\tau_S < T < t - \tau_S$),

$$\begin{aligned} S1 &= \int_n^m \frac{1}{\tau_S^2}(2\tau_S - t + T)\frac{2}{\pi\tau_R}\sqrt{\frac{\tau_R - T}{T}}dT \\ &= \int_n^m \frac{1}{\tau_S^2}(2\tau_S - t)\frac{2}{\pi\tau_R}\sqrt{\frac{\tau_R - T}{T}}dT + \int_n^m \frac{1}{\tau_S^2}T\frac{2}{\pi\tau_R}\sqrt{\frac{\tau_R - T}{T}}dT \\ &= K(2\tau_S - t)\left[\sqrt{(\tau_R - T)T} + \tau_R \arcsin\sqrt{\frac{T}{\tau_R}}\right]_n^m \\ &\quad + K\left[\frac{(2T + 3\tau_R)}{4}\sqrt{(\tau_R - T)T} - \frac{3\tau_R^2}{4}\arctan\sqrt{\frac{T}{\tau_R - T}}\right]_{\tau_R - m}^{\tau_R - n} \end{aligned} \tag{A6}$$

where

$$K = \frac{2}{\pi\tau_R\tau_S^2} \tag{A7}$$

and

$$m = \begin{cases} t - \tau_S & \text{for } \tau_S < t < \tau_R + \tau_S \\ \tau_R & \text{for } \tau_R + \tau_S < t < 2\tau_S \end{cases} \tag{A8}$$

$$n = \begin{cases} 0 & \text{for } t < 2\tau_S \\ t - 2\tau_S & \text{for } 2\tau_S < t < \tau_R + 2\tau_S \end{cases} \tag{A9}$$

For the second range ($t - \tau_S < T < t$),

$$\begin{aligned} S2 &= \int_{n'}^{m'} \frac{1}{\tau_S^2}(t - T)\frac{2}{\pi\tau_R}\sqrt{\frac{\tau_R - T}{T}}dT \\ &= Kt\left[\sqrt{(\tau_R - T)T} + \tau_R \arcsin\sqrt{\frac{T}{\tau_R}}\right]_{n'}^{m'} \\ &\quad - K\left[\frac{(2T + 3\tau_R)}{4}\sqrt{(\tau_R - T)T} - \frac{3\tau_R^2}{4}\arctan\sqrt{\frac{T}{\tau_R - T}}\right]_{\tau_R - m'}^{\tau_R - n'} \end{aligned} \tag{A10}$$

where

$$m' = \begin{cases} t & \text{for } 0. < t < \tau_R \\ \tau_R & \text{for } \tau_R < t < \tau_R + \tau_S \end{cases} \tag{A11}$$

$$n' = \begin{cases} 0. & \text{for } t < \tau_S \\ t - \tau_S & \text{for } \tau_S < t < \tau_R + \tau_S \end{cases} \tag{A12}$$

Therefore, the final integrations are as follows: If $\tau_R > 2\tau_S$,

$$S(t) = K \begin{cases} 0 & \text{for } t < 0 \\ (C1 + C2) & \text{for } 0 < t < \tau_S \\ (C1 - C2 + C3) & \text{for } \tau_S < t < 2\tau_S \\ (C1 + C3 + C4) & \text{for } 2\tau_S < t < \tau_R \\ (C5 + C3 + C4) & \text{for } \tau_R < t < \tau_R + \tau_S \\ (C4 + C6) & \text{for } \tau_R + \tau_S < t < \tau_R + 2\tau_S \\ 0 & \text{for } \tau_R + 2\tau_S < t \end{cases} \tag{A13}$$

And if $\tau_S < \tau_R < 2\tau_S$,

$$S(t) = K \begin{cases} 0 & \text{for } t < 0 \\ (C1 + C2) & \text{for } 0 < t < \tau_S \\ (C1 - C2 + C3) & \text{for } \tau_S < t < \tau_R \\ (C5 + C3 - C2) & \text{for } \tau_R < t < 2\tau_S \\ (C5 + C3 + C4) & \text{for } 2\tau_S < t < \tau_R + \tau_S \\ (C4 + C6) & \text{for } \tau_R + \tau_S < t < \tau_R + 2\tau_S \\ 0 & \text{for } \tau_R + 2\tau_S < t \end{cases} \tag{A14}$$

where

$$C1 = (\frac{1}{2}t + \frac{1}{4}\tau_R)\sqrt{t(\tau_R - t)} + (t\tau_R - \tau_R^2)\arcsin\sqrt{\frac{t}{\tau_R}} - \frac{3}{4}\tau_R^2 \arctan\sqrt{\frac{\tau_R - t}{t}} \quad \text{(A15)}$$

$$C2 = \frac{3}{8}\pi\tau_R^2 \quad \text{(A16)}$$

$$C3 = \left(\tau_S - t - \frac{1}{2}\tau_R\right)\sqrt{(t - \tau_S)(\tau_R - t + \tau_S)} + \tau_R(2\tau_R - 2t + 2\tau_S)\arcsin\sqrt{\frac{t - \tau_S}{\tau_R}} + \frac{3}{2}\tau_R^2 \arctan\sqrt{\frac{\tau_R - t + \tau_S}{t - \tau_S}} \quad \text{(A17)}$$

$$C4 = \left(-\tau_S + \frac{1}{2}t + \frac{1}{4}\tau_R\right)\sqrt{(t - 2\tau_S)(\tau_R - t + 2\tau_S)} + \tau_R(-\tau_R + t - 2\tau_S)\arcsin\sqrt{\frac{t - 2\tau_S}{\tau_R}} - \frac{3}{4}\tau_R^2 \arctan\sqrt{\frac{\tau_R - t + 2\tau_S}{t - 2\tau_S}} \quad \text{(A18)}$$

$$C5 = \frac{\pi}{2}\tau_R(t - \tau_R) \quad \text{(A19)}$$

$$C6 = \frac{\pi}{2}\tau_R(2\tau_S - t + \tau_R) \quad \text{(A20)}$$

According to these equations the proposed source time functions $S(t)$ is parameterized through the following parameters: D_{max}, τ_S and τ_R. Using Equation (6) we can easily substitute τ_S with T_{acc} in the proposed analytical relations. Moreover, Equation (4) relates the duration of the original Yoffe function (τ_R) to the effective duration of the smoothed Yoffe (τ_R^{eff}). These relations define the dependence of the STF on the parameters D_{max}, T_{acc} and τ_R^{eff}, even if the resulting expressions are analytically complicated.

Table 1: List of dynamic rupture computation models

#	τ_S (s)	T_{acc} (s)	D_{max} (m)	v_r (km/s)	τ_R (s)	τ_R^{eff} (s)	V_{peak} (m/s)	D_c (m)	$\Delta\sigma_b$ (MPa)	T_c (s)
1	0.090	0.115	1.0	2.0	1.0	1.18	3.21	0.376	21.56	0.115
2	0.125	0.160	1.0	2.0	1.0	1.25	2.71	0.437	17.58	0.170
3	0.125	0.160	1.0	2.0	2.0	1.25	1.94	0.313	12.43	0.165
4	0.150	0.195	1.0	2.0	1.0	1.30	2.47	0.475	15.96	0.205
5	0.175	0.225	1.0	2.0	1.0	1.35	2.27	0.509	14.80	0.250
6	0.175	0.225	1.0	2.0	1.5	1.85	1.87	0.421	12.10	0.245
7	0.175	0.225	1.0	2.0	2.0	2.35	1.63	0.366	10.48	0.245
8	0.175	0.225	1.0	2.0	2.5	1.85	1.46	0.330	9.38	0.245
9	0.175	0.225	1.0	2.0	3.0	3.35	1.34	0.301	8.56	0.245
10	0.175	0.225	1.0	1.5	1.0	1.35	2.27	0.501	23.56	0.240
11	0.175	0.225	1.0	1.8	1.0	1.35	2.28	0.506	18.22	0.238
12	0.175	0.225	1.0	1.9	1.0	1.35	2.27	0.508	16.10	0.240
13	0.175	0.225	1.0	2.2	1.0	1.35	2.27	0.505	14.31	0.280
14	0.175	0.225	1.0	2.3	1.0	1.35	2.27	0.512	12.36	0.275
15	0.175	0.225	1.0	2.5	1.0	1.35	2.27	0.505	12.07	0.285
16	0.175	0.225	1.0	2.7	1.0	1.35	2.27	0.498	10.84	0.270
17	0.175	0.225	1.0	3.0	1.0	1.35	2.27	0.470	10.44	0.290
18	0.250	0.320	1.0	2.0	1.0	1.50	1.88	0.597	12.77	0.375
19	0.250	0.320	2.0	2.0	1.0	1.50	3.75	1.193	25.53	0.375
20	0.250	0.320	3.0	2.0	1.0	1.50	5.63	1.790	38.30	0.375
21	0.250	0.320	1.0	2.5	1.0	1.50	1.88	0.587	10.61	0.400
22	0.300	0.385	1.0	2.0	1.0	1.60	1.70	0.640	11.91	0.455
23	0.350	0.445	1.0	2.0	1.0	1.70	1.56	0.684	11.25	0.545

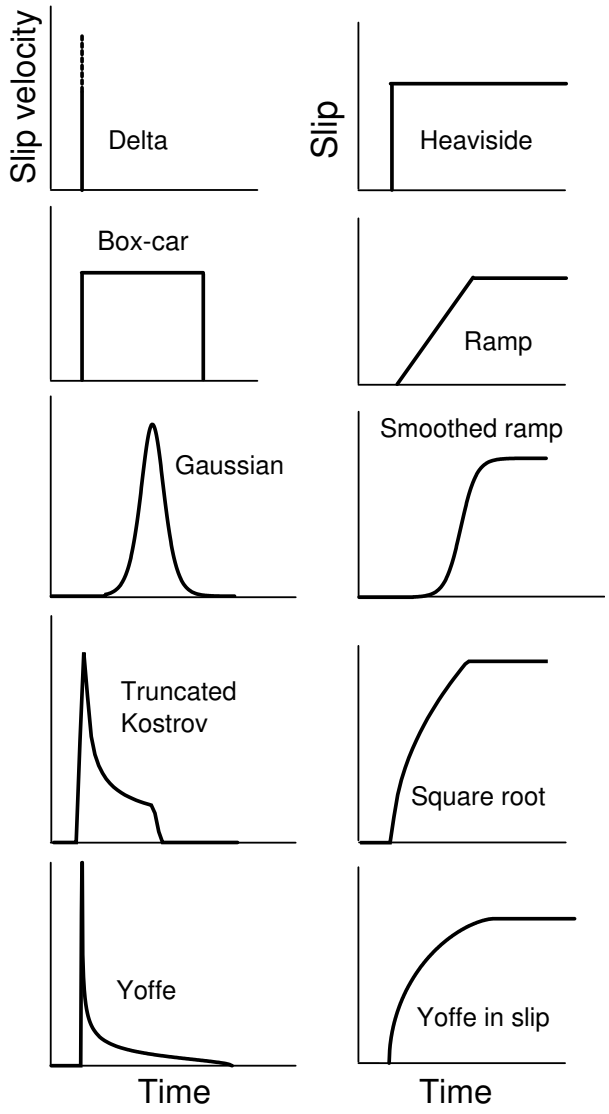

Figure 1: Slip velocity functions of delta, box-car, Gaussian, truncated Kostrov, and Yoffe are shown in left panels. The corresponding slip functions of Heaviside, ramp, smoothed ramp, square root, Yoffe in slip are shown in right panels.

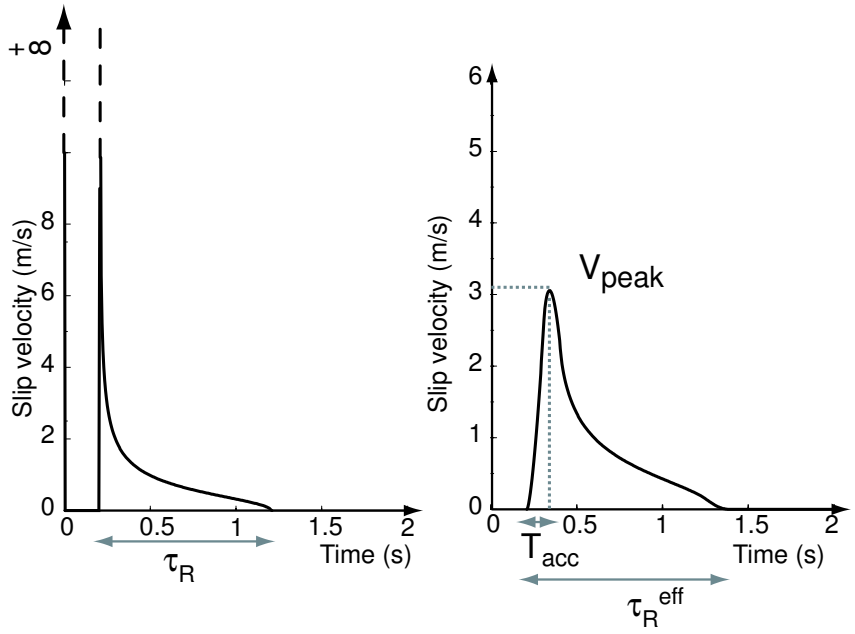

Figure 2: Comparison between the original Yoffe function (left) and the regularized Yoffe function (right) calculated for $\tau_S = 0.15s$. The peak velocity (V_{peak}) becomes finite in the smoothed case although it is infinite in the original definition.

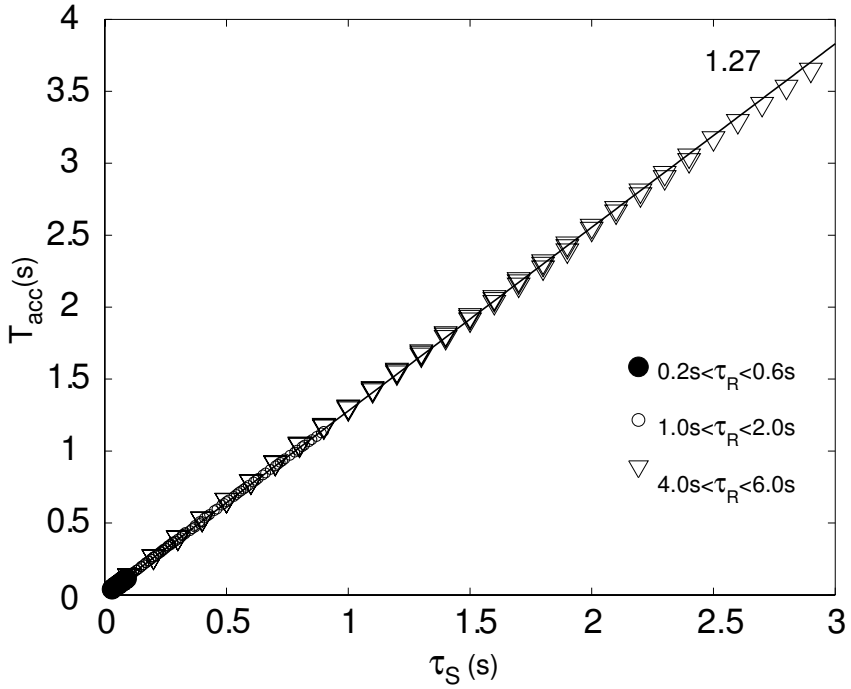

Figure 3: Correlation plot between smoothing time window (τ_S) and time to peak slip velocity (T_{acc}) for various rise time values τ_R comprised between $0.2s$ and $6.s$. The straight line represents the linear regression.

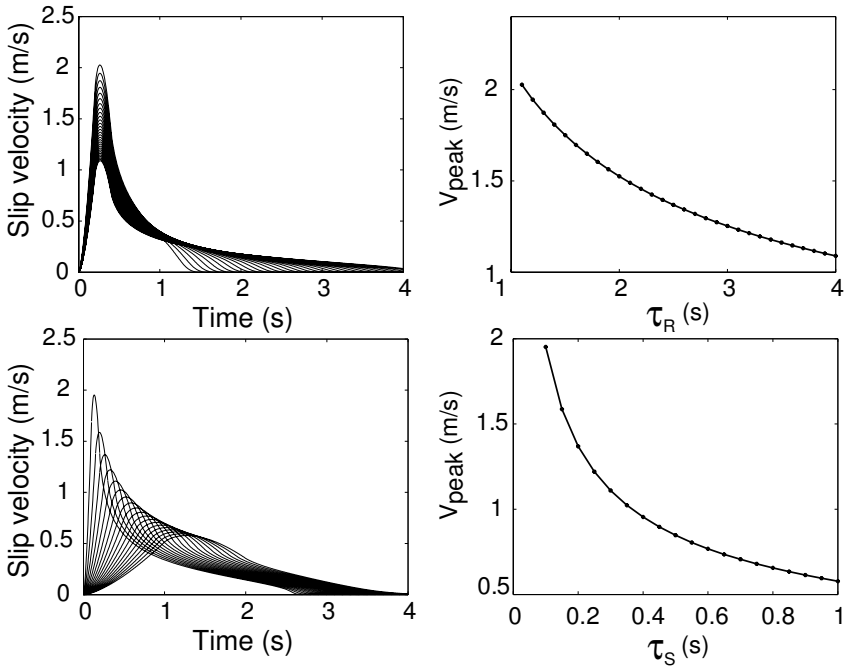

Figure 4: Upper left panel shows slip velocity functions using $\tau_S = 0.2s$ with variable τ_R in a range between $1s$ and $4s$. Lower left panel is slip velocity functions using $\tau_R = 2.5s$ with variable τ_S in a range between $0.1s$ and $1s$. In the right panels, the corresponding V_{peak} distributions as a function of τ_R or τ_S are shown.

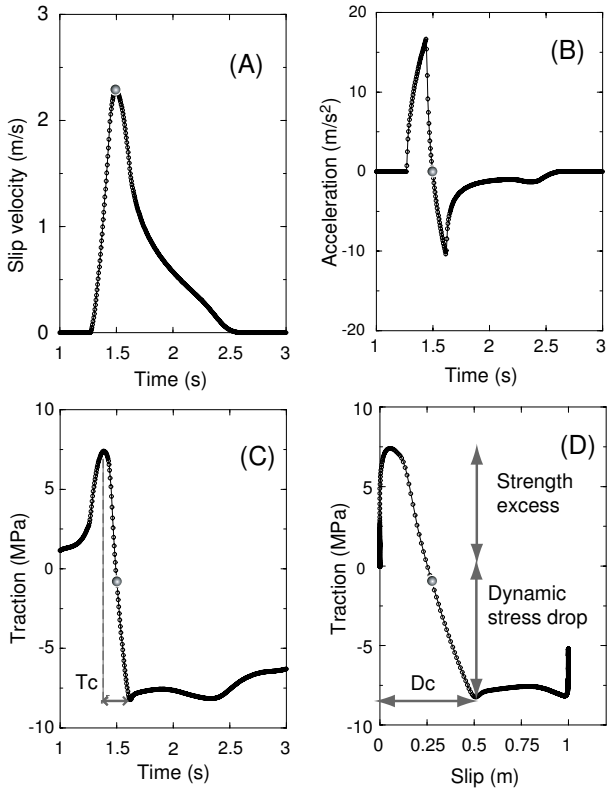

Figure 5: A typical example of (A) slip velocity, (B) slip acceleration, and (C) stress evolution as a function of time during the rupture. (D) stress evolution as a function of slip is also shown. The big open circle indicates the time of peak slip velocity ($t = T_{acc}$). [model #5 in Table 1]

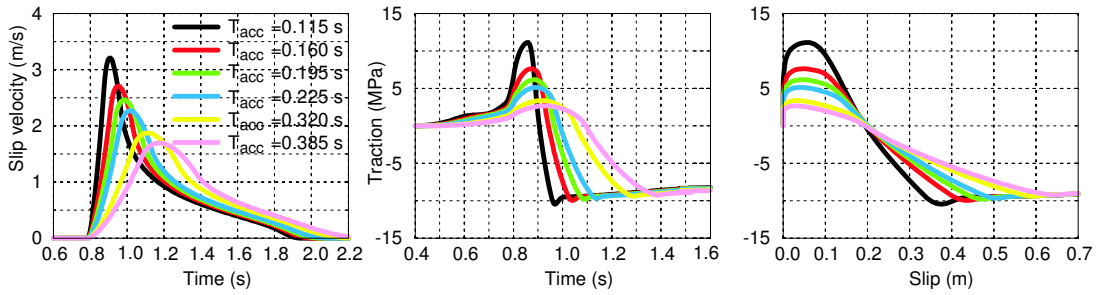

Figure 6: (left) Slip velocity evolutions, (middle) traction evolutions, and (right) constitutive behaviors for various T_{acc}. [models #1; #2; #4; #5; #21 and #22 in Table 1]

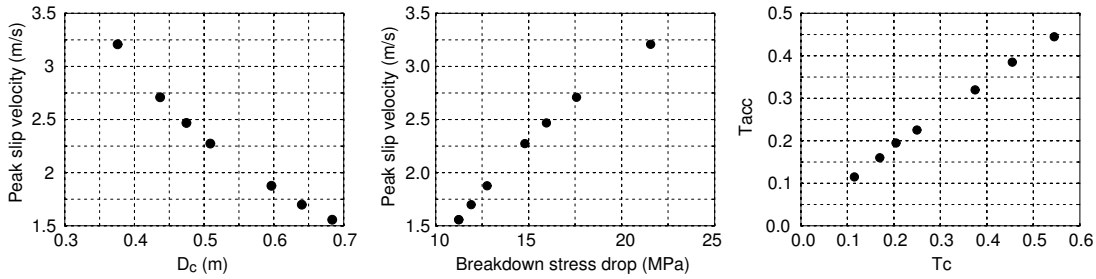

Figure 7: Relations between V_{peak} and D_c (left) or $\Delta\sigma_b$ (center) with different T_{acc} are shown. Relation between T_{acc} and T_c is also shown in right panel. [models #1; #2; #4; #5; #21; #22 and #23 in Table 1]

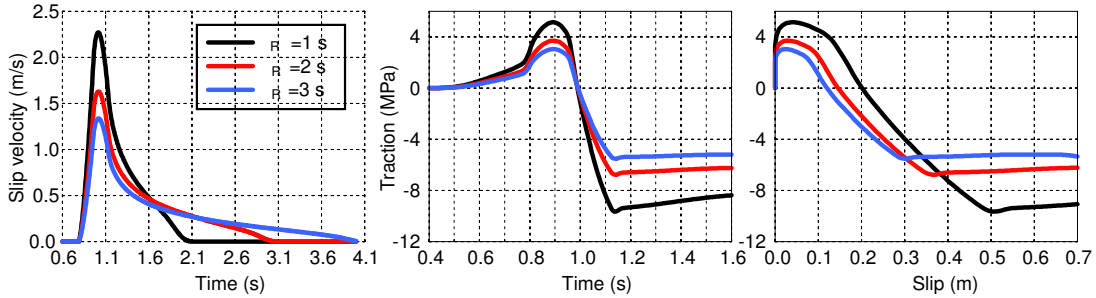

Figure 8: (left) Slip velocity evolutions, (center) traction evolution, (right) constitutive behaviors for various τ_R, using $T_{acc} = 0.225s$. [models #5; #7 and #9 in Table 1]

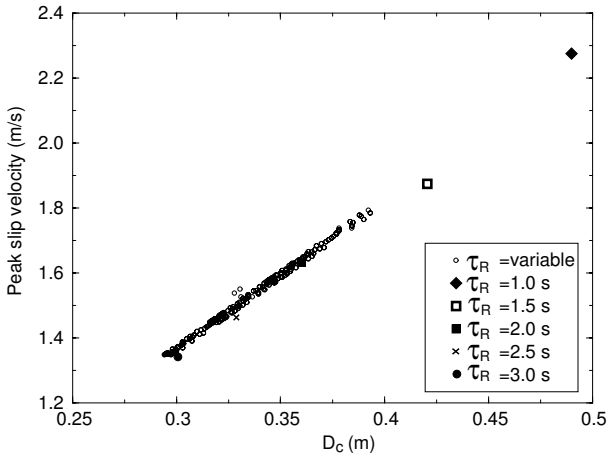

Figure 9: Relation between V_{peak} and D_c for different τ_R, assuming $T_{acc} = 0.225s$. Each black dot corresponds to different point on the fault for variable τ_R. [models #5; #6; #7; #8 and #9 in Table 1]

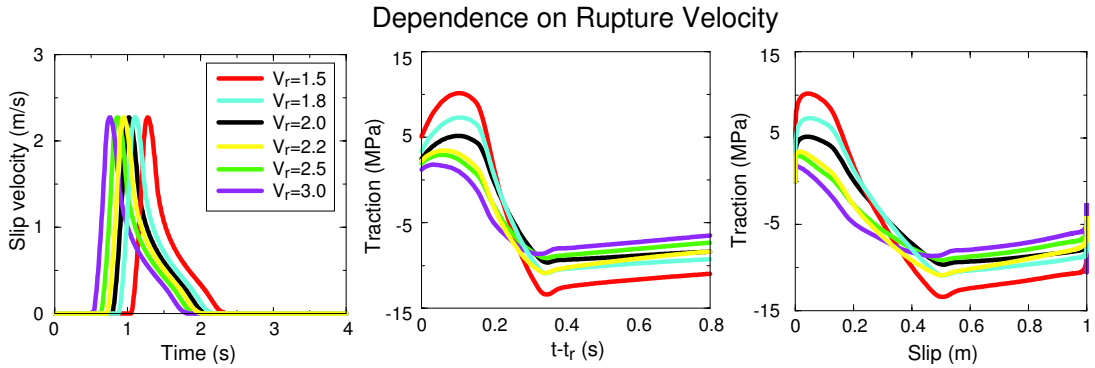

Figure 10: (left) slip velocity evolutions, (center) traction evolutions, and (right) constitutive behaviors are shown with different rupture velocities. [models #5; #10; #11; #13; #15 and #17 in Table 1]

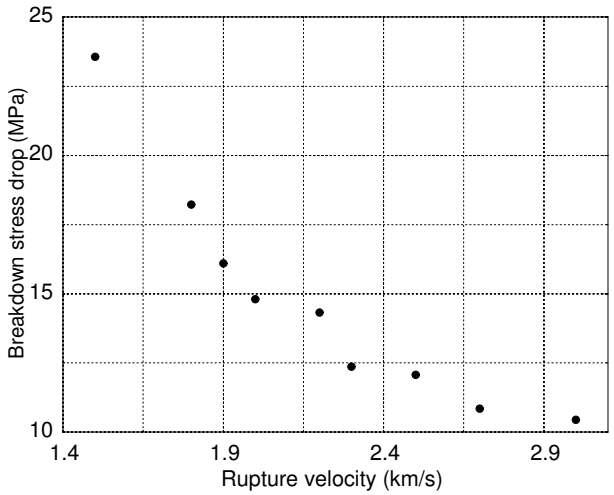

Figure 11: Relation between $\Delta\sigma_b$ and v_r, assuming $T_{acc} = 0.225s$ and $\tau_R = 1s$. [models #5; #10-17 in Table 1]